PCCP

PAPER

View Article Online
View Journal | View Issue

Cite this: *Phys. Chem. Chem. Phys.*, 2014, **16**, 1639

Determining the storage, availability and reactivity of NH_3 within Cu-Chabazite-based Ammonia Selective Catalytic Reduction systems†

I. Lezcano-Gonzalez,[ab] U. Deka,[ab] B. Arstad,[c] A. Van Yperen-De Deyne,[de] K. Hemelsoet,[de] M. Waroquier,[de] V. Van Speybroeck,[de] B. M. Weckhuysen*[b] and A. M. Beale*[b]

Received 30th September 2013,
Accepted 27th November 2013

DOI: 10.1039/c3cp54132k

www.rsc.org/pccp

Three different types of NH_3 species can be simultaneously present on Cu^{2+}-exchanged CHA-type zeolites, commonly used in Ammonia Selective Catalytic Reduction (NH_3-SCR) systems. These include ammonium ions (NH_4^+), formed on the Brønsted acid sites, $[Cu(NH_3)_4]^{2+}$ complexes, resulting from NH_3 coordination with the Cu^{2+} Lewis sites, and NH_3 adsorbed on extra-framework Al (EFAl) species, in contrast to the only two reacting NH_3 species recently reported on Cu-SSZ-13 zeolite. The NH_4^+ ions react very slowly in comparison to NH_3 coordinated to Cu^{2+} ions and are likely to contribute little to the standard NH_3-SCR process, with the Brønsted groups acting primarily as NH_3 storage sites. The availability/reactivity of NH_4^+ ions can be however, notably improved by submitting the zeolite to repeated exchanges with Cu^{2+}, accompanied by a remarkable enhancement in the low temperature activity. Moreover, the presence of EFAl species could also have a positive influence on the reaction rate of the available NH_4^+ ions. These results have important implications for NH_3 storage and availability in Cu-Chabazite-based NH_3-SCR systems.

Introduction

The emission of nitrogen oxides (NO_x), produced through the combustion of fossil fuels, is a major concern for today's society, and is subject to stringent environmental and public health protection regulations. Until now, many efforts have been made to fulfil these legislative requirements, optimizing the performance of either combustion control or post-combustion abatement technologies. In particular Ammonia Selective Catalytic Reduction (NH_3-SCR) has emerged as an effective technology for reducing NO_x emissions from oxygen-rich exhausts, typical of diesel engines, to levels required by emission regulations.[1,2]

In the last few years, many metal-promoted zeolites have been shown to be active for the NH_3-SCR reaction, with BEA, FAU and MFI-type zeolites being the most extensively studied.[1,2] Recently, it has been reported that Cu^{2+}-exchanged zeolites based on the CHA topology exhibit a superior catalytic activity and hydrothermal stability over other zeolitic structures, particularly those of the SSZ-13 form, with a lower Al content.[3–6] These improvements are attributed to the preferential location of Cu^{2+} ions in the plane of the 6-ring of the double 6-ring (D6R) unit, coordinated to three framework oxygen atoms,[5–8] which are active for NH_3-SCR.[5–8]

In addition to the metallic active species, the overall framework acidity of the catalyst material has been suggested to be a decisive factor for NH_3-SCR activity; however, the role played by the different types of acid sites in NH_3-SCR is still not fully understood. It is generally assumed that NH_3 is activated on the Brønsted sites of the zeolite in the form of ammonium ions (NH_4^+), which further react with the surface NO_x species to form N_2 and H_2O.[9–11] However, it has also been proposed that Brønsted acidity may not be required for adsorbing or activating NH_3 and that the support acts mainly as a reservoir for NH_3, which can migrate to the active site.[12–14]

Overall, NH_3 storage capacity plays a crucial role in the NH_3-SCR reaction, with NO_x conversion efficiency being to a large extent determined by the amount of stored NH_3, especially at low temperatures.[15] Though zeolites present an exceptional NH_3 storage capacity when compared with commercial vanadia-based

[a] *Materials innovation institute (M2i), Mekelweg 2, 2628 CD Delft, The Netherlands*
[b] *Inorganic Chemistry and Catalysis Group, Debye Institute for Nanomaterials Science, Utrecht University, Universiteitsweg 99, 3584 CG, The Netherlands. E-mail: a.m.beale@uu.nl, b.m.weckhuysen@uu.nl*
[c] *SINTEF Materials and Chemistry, Forskningsveien 1, N-0314 Oslo, Norway*
[d] *Center for Molecular Modelling (CMM), Ghent University, Technologiepark 903, B-9052, Zwijnaarde, Belgium*
[e] *QCMM-alliance, Ghent-Brussels, Belgium*

† Electronic supplementary information (ESI) available: Details on the theoretical calculations; and XRD, ^{27}Al MAS NMR, UV-Vis-NIR DRS, EXAFS, N_2 adsorption and SEM data of Cu-SSZ-13 zeolites. See DOI: 10.1039/c3cp54132k

catalysts,[16] an optimal performance of the NH_3-SCR unit can only be achieved by adopting an appropriate approach for NH_3 storage control. NH_3 can be released from the SCR unit by thermal desorption, combustion or reaction with NO_x; NH_3 combustion leads to the unexpected release of NO_x and/or N_2O, whereas desorption results in undesirable NH_3 emissions to the atmosphere, termed 'NH_3 slip'.[15,16] In real vehicle operation, NH_3 slip usually occurs under transient conditions, *i.e.* when the engine operation is changed. Consequently, engine speed and load fluctuations, and thus variations in flow, temperature and feed gas compositions, have to be considered to achieve a precise control of the NH_3 injection rate.[15,16] An insufficient injection may result in unacceptably low NO_x conversions, whereas an injection rate that is too high may lead to unwanted NH_3 emissions during temperature fluctuations. This is of particular importance at high temperatures, since the maximum NH_3 storage capacity reduces with increasing temperature.[15,16]

To get a deeper understanding of NH_3 storage and availability in Cu-CHA NH_3-SCR systems, the type and nature of NH_3 species adsorbed on the acid sites of the zeolite need to be identified, as well as their contribution to NH_3 storage, slip and reaction. This knowledge is essential not only for meeting future legislative requirements, but also for achieving an optimal performance of the SCR unit, leading to the development of a suitable NH_3 storage control strategy.

In a very recent work,[17] the application of Diffuse Reflectance Infra-Red Fourier Transform Spectroscopy (DRIFTS) has shown the formation of two reacting ammonia species within a Cu-SSZ-13 zeolite: namely Brønsted and Lewis acid site-adsorbed NH_3, also observed within Cu-SAPO-34, a silicoaluminophosphate material based on the CHA topology.[14,18] Due to the lower adsorption temperature, weakly-bound NH_3 species were also observed on Cu-SAPO-34,[14] including NH_3 adsorbed on silanol groups, not present at the reaction temperature. Nevertheless, very little information was obtained on the type and nature of the species formed from the interaction with either the Cu^{2+} Lewis or the Brønsted acid sites; the characteristic features of the resulting complexes were not completely assigned, whereas the possible contribution of extra-framework Al (EFAl) species, also with Lewis acid character, to the Lewis acid site-adsorbed NH_3 was not considered[17,18] and therefore not investigated.[14] Furthermore, the Cu-SSZ-13 zeolite was activated under inert flow,[17] leading to Cu^{2+} self-reduction[19–21] and resulting in changes in the acid strength of the Brønsted acid sites, as observed for vacuum activated Cu-SSZ-13 samples.[21] Clearly, this could affect the adsorption properties of the zeolite.

In the present investigation, the type and nature of NH_3 species adsorbed on CHA-type zeolites and their evolution during standard SCR has been investigated by combining *in situ* Fourier Transform Infra-Red (FTIR) Spectroscopy with DFT-based simulations, as well as temperature programmed desorption (TPD) of NH_3. As catalysts, five CHA-type zeolites have been used, presenting different populations of acid sites, *i.e.* Brønsted acid sites, Cu^{2+} ions and/or EFAl species, characterised by X-ray diffraction (XRD), ^{27}Al MAS NMR, chemical analysis, UV-Vis-NIR DRS, X-ray absorption spectroscopy (XAFS), N_2 adsorption and scanning electron microscopy (SEM), as well as FTIR and theoretical calculations. The combination of theory and experiment on a systematic set of samples enabled us to unambiguously identify not two, but three types of NH_3 species within Cu-CHA-based zeolites (*i.e.* NH_4^+ ions formed on the Brønsted acid sites; $[Cu(NH_3)_4]^{2+}$ complexes and NH_3 adsorbed on EFAl species), with a complete assignment of the typical bending vibrations of these complexes. The results here presented give therefore, further insight into previous works, with a basis for future data interpretation. Moreover, based upon results outlined here, evidence is given concerning the role of these species on NH_3 storage, availability and reactivity, as well as suggestions with regard to the important problem of NH_3 slip. Importantly, a catalyst exhibiting an enhanced NH_3 availability is also presented.

Experimental

Catalysts

Two different H-form CHA-type zeolites were employed as parent materials; *i.e.* low silica H-CHA (Si/Al = 2.2) and high silica H-SSZ-13 (Si/Al = 15) zeolites. Low silica H-CHA zeolite was provided by Tosoh, whereas Al-containing SSZ-13 zeolite was synthesized as described previously, but using static conditions.[22] The sample was calcined in air with the following temperature program: 1 °C min^{-1} to 120 °C, held for 2.5 h; 2.2 °C min^{-1} to 350 °C, and 3 h at this temperature; and finally 0.8 °C min^{-1} to 580 °C, and held for 3 h. Identity and purity of the zeolite were verified by XRD (Bruker D2 phaser).

The studied Cu-zeolites were labelled as follows: Cu-SSZ-13(x), with x being the degree of Cu^{2+} exchange in %. Cu-SSZ-13(67) and Cu-CHA were prepared *via* wet ion exchange (WIE) of the calcined parent zeolite, using an aqueous solution of copper sulphate. Typically, 50 ml of a 0.1 M solution of $CuSO_4$ (Merck, 99%) was mixed with 1 g of the zeolite and magnetically stirred for 2 h at 80 °C. The product was then recovered by vacuum filtration, washed with deionised water, and dried at 120 °C overnight. The resulting sample was calcined in air with the following temperature program: 2 °C min^{-1} to 120 °C, held for 30 min; and finally 1 °C min^{-1} to 550 °C, and 4 h at this temperature. Cu-SSZ-13(100) was prepared *via* three successive ion exchanges of the parent Cu-SSZ-13(67), following the procedure reported above.

Catalyst characterisation

XRD patterns of as-synthesized, calcined and Cu-exchanged samples were recorded on a Bruker D2 X-ray powder diffractometer equipped with a Co Kα X-ray tube (λ = 1.7902 Å). The crystal size and morphology was analysed by SEM using a Tecnai FEI XL 30SFEG microscope. Pore volumes and BET surface areas were determined by nitrogen sorption measurements using a Micromeritics ASAP 2420. The chemical analysis was performed by coupled plasma optical emission spectrometry (ICP-OES, Perkin-Elmer 3300DV instrument). UV-Vis-NIR DRS was collected using a Varian Cary 500 UV-Vis-NIR spectrometer equipped with a DRS accessory to

allow collection in the diffuse reflectance mode. Spectra were collected between 5000–50 000 cm^{-1} with a data interval of 10 cm^{-1} and at a rate of 6000 cm^{-1} min^{-1}. XAFS measurements were performed at the Dutch-Belgian beamline (DUBBLE; BM26A) in the European Synchrotron Research Facility (ESRF), Grenoble, France. A detailed description of the beamline can be found elsewhere.[23] A Si(111) double crystal monochromator and Si/Pt mirrors were used for harmonic rejection. XAFS data (X-ray absorption near edge (XANES) and extended X-ray absorption fine structure (EXAFS)) at the Cu K-edge (8979 eV) was collected in transmission mode in quick scanning mode (XANES with 1 eV steps/500 ms integration time with scanning over the EXAFS region utilising steps of increasing size 1–4 eV and integration times 1–3 s resulting in a total acquisition time of ~40 min). Typically 3 scans were recorded per sample. The X-ray absorption data were background corrected using Athena (IFFEFIT software package).[24] The normalized data were k^3-weighed and a least-squares fitting analysis was performed in a k-range of 3–10 Å. The FTs of the k^3-weighed data were phase corrected and fit to the proposed theoretical model using the DL-EXCURV program.[25] ^{27}Al MAS NMR experiments were carried out on a Bruker Avance AV III 500 WB spectrometer using a 3.2 mm triple resonance MAS probe with the sample spinning at 20 kHz. The one-dimensional spectra were recorded upon single-pulse $\pi/12$ excitation with a pulse duration of 0.44 μs. The ^{27}Al chemical shifts are referenced to an aqueous solution of 1 M $Al(NO_3)_3$ (0 ppm). Simulation of the spectra was performed with DMFIT software.[26]

Infrared spectroscopy

FTIR spectra were collected with a Perkin-Elmer Spectrum One FTIR spectrometer, using self-supported wafers of *ca.* 5 mg. Spectra were obtained by accumulating 5 scans at a spectral resolution of 4 cm^{-1}. Prior to the experiment, the zeolite pellet was pre-treated for 12 h with 10% O_2 in He at 250 °C. After the pre-treatment, the catalyst was exposed to 1000 ppm NH_3 at 250 °C over a period of 30 min. Subsequently, the catalyst was exposed to He for 5 min, and then to a mixture of NO and O_2 (1000 ppm NO and 5% O_2) at 250 °C.

Temperature programmed desorption

Temperature programmed desorption of ammonia (NH_3-TPD) was performed making use of a mass spectrometer (MS, Hiden Analytical, HPR-20 QIC). 150 mg of sample was outgassed at 600 °C for 1 h with 10% O_2 in He, followed by NH_3 adsorption at 100 °C for 1 h (13 ml min^{-1}; 5% NH_3 in He). Subsequently, the sample was flushed with He for 1.5 h at 100 °C to remove physically adsorbed NH_3. NH_3 desorption was carried out by rising the temperature to 670 °C with a heating rate of 5 °C min^{-1}.

Catalyst testing

Catalytic tests were performed in a fixed bed plug flow set up. Typically, 150 mg of powdered catalyst material (sieve fractions of 0.425–0.150 mm) was loaded in a 1 cm OD quartz tubular reactor. Prior to the experiment, the zeolite sample was pre-treated for 1 h with 5% O_2 in He at 550 °C. After the pre-treatment, the desired reaction temperature was fixed and then, the catalyst exposed to a SCR feed composition of 1000 ppm NO, 1000 ppm NH_3 and 5% O_2, and He for balance, with a Gas Hourly Space Velocity (GHSV) of 100 000 h^{-1}. Steady-state measurements were performed at different temperatures, from 100 to 600 °C, using a stabilisation period of 30 min at each temperature and analysing the output gases by mass spectrometry (Hiden Analytical, HPR-20 QIC). All SCR gases were provided by Linde. To avoid condensation in the reaction system, all the gas lines were heated to 150 °C.

Theoretical calculations

First-principles simulations on Cu- and H-exchanged SSZ-13 zeolites were performed using the QUICKSTEP module in the CP2K software program.[27–29] For the majority of calculations, plane wave density functional theory (DFT) calculations were carried out using the Gaussian Plane Wave (GPW) method. The BLYP exchange–correlation functional,[30,31] in combination with a double-zeta MOLOPT basis set[32] and plain wave cutoff of 300 Ry was used. For the geometry optimisations, atoms near the reactive center (*i.e.* in the D6R) were treated with Gaussian Augmented Plane Waves (GAPW) and an Ahlrichs pTZV basis set.[33] Molecular Dynamics (MD) simulations were performed on all atoms. After 2 ps equilibration with the canonical sampling through velocity rescaling thermostat,[34] the more robust Nosé–Hoover thermostat[35] was used for 13 ps with a timestep of 0.5 fs for the Cu-containing zeolites while the protonated SSZ-13 were all simulated for 32 ps with the same time step. The temperature of the simulations was held to 600 K in accordance with experiment. All post-processing of the MD simulations was done using the program MD-tracks.[36] IR properties were calculated using a Fourier-based technique with input from the MD simulations.[37] More details are given in the ESI.† In addition, IR data resulting from a static Normal Mode Analysis (NMA) on the optimized geometries are included in the ESI.† The computed harmonic frequencies are compared with the experimental data; in order to get a good quantitative agreement, scaling factors can be applied.[38] In the present work, our main interest is a good qualitative correlation, and hence the reported theoretical data are non-scaled.

The unit cell parameters were taken from crystallographic data of pure siliceous SSZ-13 and kept fixed during the optimisation. The CHA unit cell contains 36 T-sites with corresponding oxygen atoms. For both the Cu-SSZ-13 and H-SSZ-13 simulations a double Si to Al substitution was assumed. This results in unit cells containing 109 ($1Cu^{2+}$) and 110 ($2H^+$) atoms without NH_3 adsorbed and cells containing 113 and 114 atoms when NH_3 is adsorbed to the active site. Model containing a $[Cu^{2+}(OH)^-]^{2+}$ and $[Cu(NH_3)_4]^{2+}$ complex in the center of the CHA cage were also considered.

Results and discussion

The catalysts

Table 1 summarises the chemical composition of the zeolite materials used here as catalysts. The elemental analysis of

Table 1 Chemical analysis of the zeolites used as catalyst materials in the present study

Sample	Si/Al	Cu loading (wt%)	I.E.[a] (%)	EFAl[b] (%)
H-SSZ-13	15	—	—	—
Cu-SSZ-13(67)	15	2.0	67	5.3
Cu-SSZ-13(100)	22	2.5	100	n.d.[c]
H-CHA	2.2	—	—	18
Cu-CHA	2.2	4.9	39	18

[a] Ion exchange level (I.E.); normalised to 100% for a Cu to Al ratio of 1 : 2. [b] Determined by ^{27}Al MAS NMR (see ESI; Fig. S1). [c] Not detected.

Cu-SSZ-13(67) and Cu-CHA zeolites reveal varying Cu^{2+}-exchange levels, which can be related to the different Si/Al ratio and hence, to the different population of Brønsted acid sites in the H-form parent materials. Furthermore, the ^{27}Al MAS NMR data show the presence of different amounts of EFAl species, attributed to the different synthesis method and/or Al content of the parent materials. No effect on the Si/Al ratios was found as a result of the Cu^{2+}-exchange treatments.

The results obtained for the Cu-SSZ-13(100) zeolite indicate an increase of 25% in the Cu content after the successive exchanges, reaching a final loading of 2.5 wt%, which corresponds to the maximum ion exchange level (I.E. = 100%) of the zeolite. In addition, the results show a slightly larger Si/Al ratio, indicating that mild dealumination takes place during successive exchanges with Cu^{2+}. It should be noted, however, that no EFAl species were detected by ^{27}Al MAS NMR (see Table 1 and Fig. S1, ESI†), probably due to acid leaching of these species during the successive exchanges, conducted at a pH of 3–4. Furthermore, the XRD patterns (see ESI;† Fig. S2) indicate that the crystallinity of the zeolite is maintained after the successive exchanges with Cu^{2+}.

To obtain further insight in the nature of the active sites, FTIR measurements of the dehydrated zeolites were performed and combined with DFT-based simulations of vibrational frequencies. Prior to the experiment, pre-adsorbed water molecules were removed by treating the zeolite materials for 12 h with 10% O_2 in He at 250 °C, thus preventing self-reduction of the Cu^{2+} ions.[19–21] Fig. 1 depicts the FTIR spectra of the dehydrated zeolites, acquired at 250 °C under flow conditions (10% O_2 in He). As clearly seen, the spectra show the presence of a very sharp peak, at 3735 cm^{-1}, that could be attributed to isolated internal silanol groups.[39,40] This peak becomes more evident for the Cu-SSZ-13(100) zeolite (Fig. 1c), consistent with mild dealumination occurring during the consecutive exchanges, as indicated above. No bands at 3675 cm^{-1}, corresponding to OH groups in partially extra-lattice positions,[40–43] were detected for the SSZ-13 zeolites (Fig. 1a–c), whereas for the high-silica CHA zeolites (Fig. 1d–e) this component may not be observable since it could be superimposed with other bands in the hydroxyl region.

A very broad band is found in the spectra of H-CHA and Cu-CHA zeolites, with a maximum at 3611 cm^{-1}, corresponding to Brønsted acidic OH groups. In contrast, two kinds of bridging hydroxyl groups can be observed in the spectra of the dehydrated H-SSZ-13, Cu-SSZ-13(67) and Cu-SSZ-13(100) zeolites, with bands

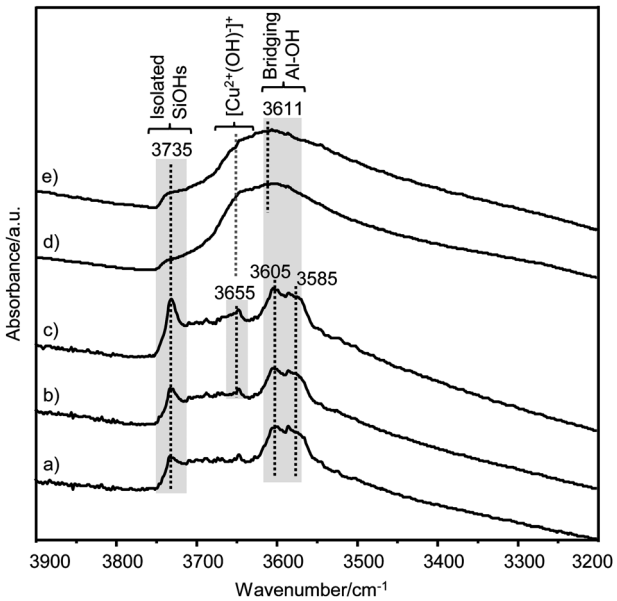

Fig. 1 FTIR spectra of H-SSZ-13 (a), Cu-SSZ-13(67) (b), Cu-SSZ-13(100) (c), H-CHA (d), and Cu-CHA (e) zeolites, activated with 10% O_2 in He, at 250 °C for 12 h.

at 3605 and 3585 cm^{-1}. It is known that CHA-type zeolites present four symmetrically non-equivalent acid OH groups, with approximately the same stability and acid strength;[43–47] three sites are part of an 8-ring connecting two cages, whereas the fourth group is in contact only with one cage. To further validate previous assignments, periodic models were constructed for the H-form SSZ-13 zeolite (see Fig. S5, ESI†), and the O(1) and O(2) sites, corresponding to the high- and low-frequency bands, respectively, were both considered; O(1) site belongs to two 4-ring and one 8-ring, whereas O(2) belongs to one 4-ring, one 6-ring and one 8-ring ring. From the MD simulations, the ν(OH) stretching frequencies for the O(1) and O(2) site were found at 3626 and 3562 cm^{-1}, respectively, in line with the experiment and with previous studies.[43–47]

Importantly, the FTIR spectrum of the zeolite with 100% exchange (see Fig. 1c), shows two intense bands of the bridging hydroxyl groups, at 3605 and 3585 cm^{-1}, comparable to those observed for the Cu-SSZ-13(67) zeolite, indicating that the Brønsted acid sites remain in the sample despite complete Cu^{2+}-exchange. This could be caused by the presence of a second type of Cu site (*i.e.* Cu oxides), not occupying the framework exchange positions, and thus requiring the presence of residual protons to ensure framework neutrality. However, the UV-Vis-NIR DRS and EXAFS data of the hydrated Cu-SSZ-13(100) zeolite (see ESI;† Fig. S7 and S8 and Table S2) show that almost all the Cu is present as isolated Cu^{2+} ions, with only a very small fraction of the Cu atoms not located in exchange positions, as CuO species. Therefore, the signal intensity attributable to Brønsted acidity in Cu-SSZ-13(100) zeolite is too large to be due to the presence of such small amount of extra-framework CuO and other possibilities should be considered, such as the presence of Cu species balanced by isolated Al atoms.[21,48–51]

In recent times, it has been proposed that two different Cu sites in CHA-type zeolites exist and that their occupation depends upon Cu exchange level; at low loadings, Cu^{2+} ions are located in the D6R units, whereas at high loadings the ions are located inside the large cages.[52–55] More recently, Giordanino *et al.* reported the presence of different Cu species on O_2 activated Cu-SSZ-13 samples (Si/Al = 13.1; Cu/Al = 0.444);[21] in addition to the well-known isolated Cu^{2+} ions, monovalent Cu^{+} and $[Cu^{2+}(OH)^{-}]^{+}$ species were also detected, for which Al pairs are not required to achieve charge compensation. The authors observed that the concentration of Brønsted sites was not affected by the activation treatment, obtaining similar intensities of the Brønsted acid sites for the samples activated in O_2 or in vacuum conditions.[21] Accordingly, no new bridging hydroxyls were created during the vacuum treatment to compensate the loss of positive charge as a result of Cu^{2+} self-reduction, and the authors concluded that not all the Cu^{2+} ions initially present were balancing the negative charge created by two Al atoms, being also probably in the form of monovalent $[Cu^{2+}(OH)^{-}]^{+}$ species.[21] The presence of $[Cu^{2+}(OH)^{-}]^{+}$ complexes was verified by using both CO and NO as probes, confirming the formation of Cu–OH···CO adducts and mono-nitrosyls, respectively. Additionally, the authors assigned the stretching OH band at 3657 cm^{-1} to the ν(OH) stretch of $[Cu^{2+}(OH)^{-}]^{+}$ complexes.[21]

Interestingly, the spectrum of the Cu-SSZ-13(100) zeolite (Fig. 1c) shows the presence of a broad band in the range from 3647 to 3666 cm^{-1}, centred at 3655 cm^{-1}, much more intense than for the Cu-SSZ-13(67) sample (Fig. 1b), suggesting the presence of monovalent $[Cu^{2+}(OH)^{-}]^{+}$ species. This could explain the excess of Brønsted acidity observed for Cu-SSZ-13(100) zeolite, for which the maximum cation exchange capacity has already been reached. To gain further insight into the origin of this band, the theoretical stretching frequency of the $[Cu^{2+}(OH)^{-}]^{+}$ complex in a CHA-type zeolite was also calculated. The computed FTIR spectrum resulting from a molecular dynamic investigation shows two peaks which represent different orientations of the OH group, corresponding to OH stretch vibrations around 3614 cm^{-1} and 3660 cm^{-1} (the optimized geometries of the complexes are shown in Fig. 2). During the simulation, the OH is mainly oriented away from the framework and no hydrogen bond is formed between the OH group and framework oxygen atoms (Fig. 2b). This corresponds to a vibrational peak at *ca.* 3660 cm^{-1}, in excellent agreement with the results here and those presented before.[21] Clearly, this result shows that not all the Cu^{2+} ions are balancing the negative charge created by two Al atoms, since some of the Cu species are present in the form of monovalent $[Cu^{2+}(OH)^{-}]^{+}$ complexes, thus resulting in a greater than expected number of Brønsted acid sites, as observed in the FTIR spectrum of the dehydrated Cu-SSZ-13(100) zeolite.

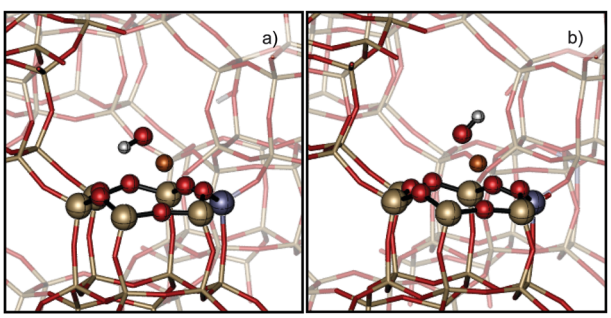

Fig. 2 Optimized structures for $[Cu^{2+}(OH)^{-}]^{+}$ complexes in SSZ-13 zeolite. Gold: Si, dark blue: Al, red: O, orange: Cu and white: H.

Identification of NH_3 species in CHA-type zeolites

As mentioned in the Introduction, the type of NH_3 species formed on Cu-SSZ-13 has been previously investigated by DRIFTS.[17] Zhu *et al.* identified two different NH_3 species; namely Brønsted acid site-adsorbed NH_3 and Lewis acid site-adsorbed NH_3. However, very little information was obtained on the type of complexes formed upon the interaction with either the Cu^{2+} or the Brønsted acid sites and the influence of EFAl species was not considered.[17] In addition, the zeolite sample was activated in flowing He, leading to some extent, to Cu^{2+} to Cu^{+} self-reduction.[19–21] This could also result in a different acid strength of the Brønsted acid sites, as previously observed for vacuum activated samples.[21] In this work, all the zeolite samples were activated with 10% O_2 in He, at 250 °C for 12 h, in order to avoid Cu^{2+} self-reduction.

The interaction of NH_3 with the bridging hydroxyl groups was modelled using OH groups at different framework positions, *i.e.* O(1) and O(2), representative of the high- and low-frequency bands, respectively (Fig. 3a and b), as described above. The optimized theoretical structures indicate that NH_3 molecules are protonated in both complexes, forming stable NH_4^{+} ions on the Brønsted hydroxyl groups of the zeolite. For the adsorption NH_3 on the Cu^{2+}-exchanged SSZ-13 zeolite, two different situations were considered; the adsorption of only one NH_3 molecule (NH_3@Cu^{2+} site; Fig. 3c), maintaining the interactions between the Cu^{2+} ions and the framework oxygen atoms, and a $[Cu(NH_3)_4]^{2+}$ complex

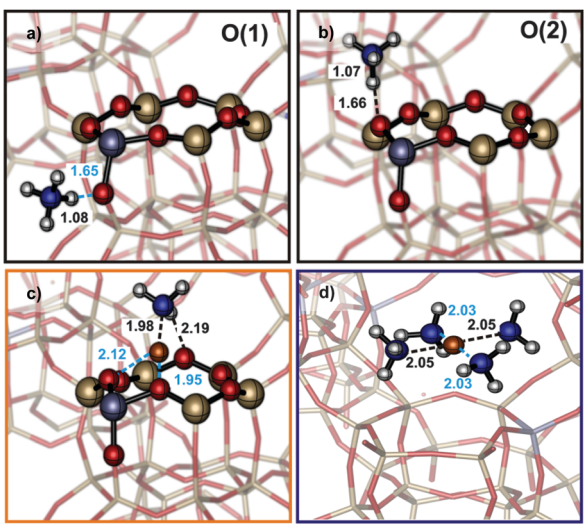

Fig. 3 Optimized structures of NH_3 on a Brønsted acid site at O(1) (a) and O(2) (b) framework positions; on a Cu^{2+} site (c) and of the $[Cu(NH_3)_4]^{2+}$ complex (d) in SSZ-13. Blue: N, gold: Si, dark blue: Al, red: O, orange: Cu and white: H. Distances are expressed in angstroms.

Table 2 Experimental and theoretical frequencies of NH_3 species formed on the acid sites of CHA-type zeolites

		ν_{theor} (cm^{-1})			
	ν_{exp} (cm^{-1})	O(1)	O(2)	Assignment	Ref.
NH_3@Brønsted site	3400–3100	3480–3200		$\nu(NH_4^+)$	11, 45, 56, 58
	1455–1448	1432	1455	$\delta(NH_4^+)_{as}$	11, 45–46, 57–58
	1401–1393	1370	1368	$\delta(NH_4^+)_{s}$	11, 45–46, 57–58
		ν_{theor} (cm^{-1})			
	ν_{exp} (cm^{-1})	$[Cu(NH_3)]^{2+}$	$[Cu(NH_3)_4]^{2+}$	Assignment	Ref.
NH_3@Cu^{2+} site	3400–3100	3480–3200		$\nu(NH_3)$ of NH_3 in $[Cu(NH_3)_4]^{2+}$	42, 56
	1619	1601	1606	$\delta(NH_3)_{as}$ of NH_3 in $[Cu(NH_3)_4]^{2+}$	42, 56–57
	—	1535	—	H-bonded $\delta(NH_3)_{as}$ in $[Cu\text{-}NH_3]^{2+}$	—
	1278	1271	1285	NH_3 wagging of NH_3 in $[Cu(NH_3)_4]^{2+}$	42, 56–57
NH_3@EFAl	1620[a]	[b]		Weakly adsorbed NH_3 on Lewis sites	59
	1332–1324	[b]		Strongly adsorbed NH_3 on EFAl	59

[a] Only detected in low silica H-CHA zeolite; overlapped in the spectra of the Cu-zeolites with the $\delta(NH_3)_{as}$ of NH_3 in $[Cu(NH_3)_4]^{2+}$. [b] Not modeled.

($(NH_3)_4$@Cu^{2+} site; Fig. 3d), centred in the zeolite cage, for which the Cu–O interactions are absent (see ESI†). Table 2 gives an overview of the assigned theoretical and experimental frequencies. The structures of the NH_3@Brønsted site (O1) and NH_3@Brønsted site (O2) complexes present two peaks in the bending region, corresponding to the symmetric and anti-symmetric vibrations of the chemisorbed NH_4^+ ions. In contrast, the structure of the NH_3@Cu^{2+} site complex presents a third IR active peak, at 1535 cm^{-1}, arising from the interaction between a hydrogen atom of NH_3 and a framework oxygen atom (see Fig. 3b). Due to the presence of different NH_3 molecules, the vibrational analysis of the $[Cu(NH_3)_4]^{2+}$ complex shows several contributing modes; the main theoretical absorbance bands, shown in Table 2, are very close to the experimental values previously obtained for this complex on Cu-containing zeolites.[42,56,57]

Fig. 4a displays the FTIR difference spectrum of the H-SSZ-13 zeolite acquired after NH_3 adsorption at 250 °C. As expected, the spectrum shows the disappearance of the bands of the bridging hydroxyl groups, at 3605 and 3585 cm^{-1}, together with the appearance of new features, at 3400–3100 and 1429 cm^{-1}, attributed to stretching[11,45,56,58] and bending[11,45,46,57,58] vibrations respectively, of NH_4^+ ions, resulting from NH_3 protonation over the Brønsted acidic hydroxyl groups (see Table 2). The band centred at 1429 cm^{-1} is a combination of two different contributions, at 1448 and 1393 cm^{-1}, which can be readily assigned to the anti-symmetric and symmetric bending vibrations of NH_4^+ ions respectively, in accordance with the theoretical calculations (see Table 1) and also with previous works.[11,45,46,57,58] Conversely, the spectra recorded for the Cu^{2+}-loaded SSZ-13 zeolites (Fig. 4b and c) show the presence of additional bands in the bending region, at 1619 and 1278 cm^{-1}, of NH_3 adsorbed over the Cu^{2+} Lewis sites of the zeolite, resulting in a $[Cu(NH_3)_4]^{2+}$ complex, in agreement with the calculated frequencies (Table 2). It is important to note that the ν(OH) stretch of $[Cu^{2+}(OH^-)]^+$ complexes is observed as a negative band after NH_3 adsorption, indicating that NH_3 molecules are also adsorbed on this particular site.

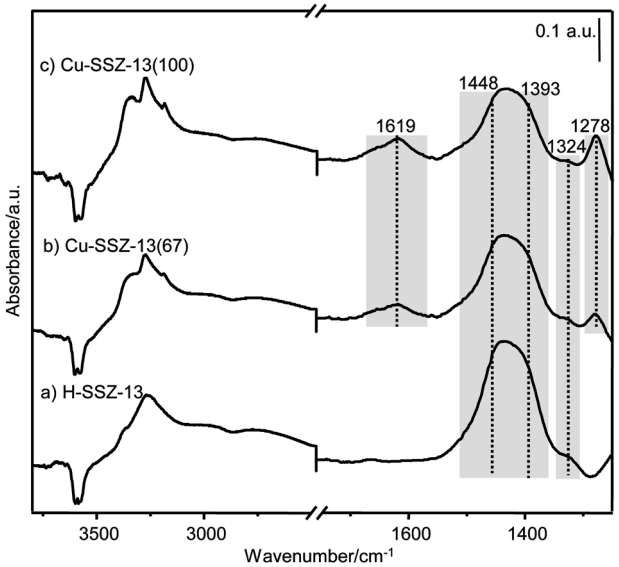

Fig. 4 FTIR difference spectra of NH_3 adsorbed on H-SSZ-13 (a), Cu-SSZ-13(67) (b), and Cu-SSZ-13(100) (c) zeolites at 250 °C. Note the presence of at least two different NH_3 species: NH_4^+ ions (1448 and 1393 cm^{-1}) and $Cu[(NH_3)_4]^{2+}$ complexes (1619 and 1278 cm^{-1}).

The interaction of NH_3 with EFAl species, also possessing Lewis acid character, can clearly be seen in the spectra of the low-silica CHA-type zeolites (Fig. 5), containing ~18% EFAl species (as seen by ^{27}Al MAS NMR; Table 1). Similarly to Cu-SSZ-13 zeolites, the spectrum of the Cu-CHA zeolite (Fig. 5b) shows the corresponding vibrations of NH_4^+ ions and $[Cu(NH_3)_4]^{2+}$ complexes, accompanied by an intense band, at 1327 cm^{-1}, attributed to NH_3 species strongly adsorbed on EFAl species.[59] In accordance, the spectrum of the H-form zeolite (Fig. 5a) also shows the presence of this band, together with the characteristic vibration of weakly adsorbed NH_3 on Lewis acid sites, at 1620 cm^{-1},[59] overlapped for Cu-CHA with the band of the $[Cu(NH_3)_4]^{2+}$ complex (Fig. 5b). Whilst the peak corresponding to strongly adsorbed NH_3 on EFAl is also present in the spectra of the Cu-SSZ-13(67) zeolite (1324 cm^{-1}, Fig. 4b),

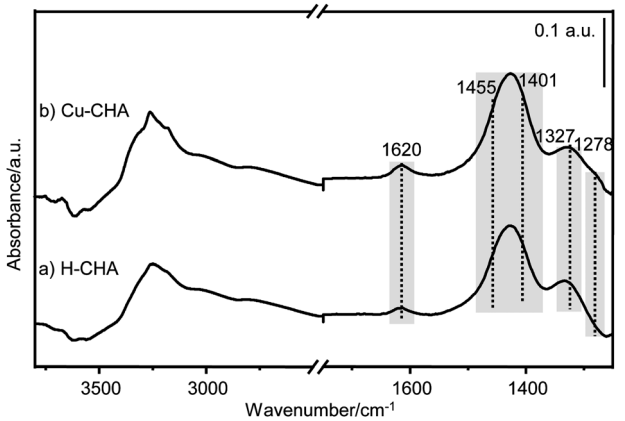

Fig. 5 FTIR difference spectra of NH_3 adsorbed on H-CHA (a), and Cu-CHA (b) zeolites at 250 °C. Note the presence of at least three different NH_3 species: NH_4^+ ions (1455 and 1401 cm^{-1}), $Cu[(NH_3)_4]^{2+}$ complexes (1620 and 1278 cm^{-1}) and NH_3 coordinated with extra-framework Al (EFAl) species (1620 and 1327 cm^{-1}).

with 5.3% of EFAl species (Table 1), the low intensity when compared with that of the Cu-CHA zeolite suggests that EFAl species barely contribute to the band at 1619 cm^{-1} for the SSZ-13 zeolites.

Therefore, three different types of NH_3 species have been found in CHA-type zeolites; NH_4^+ ions formed on the Brønsted acid sites, $[Cu(NH_3)_4]^{2+}$ complexes, resulting from NH_3 coordination with the Cu^{2+} Lewis sites, and, when present, NH_3 coordinated with EFAl species. Importantly, for completeness we observe that NH_3 molecules can also be physisorbed or weakly adsorbed at lower temperatures (see NH_3-TPD profiles below).

To provide further support to those assignments, NH_3-TPD measurements were performed. Consistent with the *in situ* FTIR results, the NH_3-TPD profiles of the high-silica Cu-SSZ-13 zeolites (Fig. 6) reveal two different desorption peaks above 250 °C (intermediate-temperature (IT) and high-temperature (HT) peaks; Fig. 6), corresponding to acid sites with different acid strength.

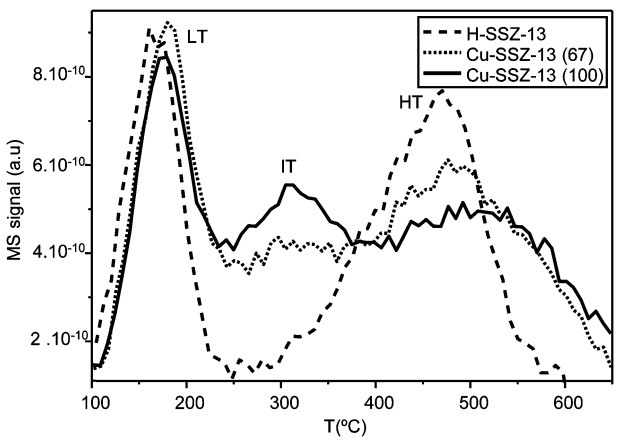

Fig. 6 NH_3-TPD profiles of H-SSZ-13, Cu-SSZ-13(67) and Cu-SSZ-13(100) zeolites. LT: low temperature peak; IT: intermediate temperature peak, and HT: high temperature peak.

In contrast, the profile of H-SSZ-13 shows only one desorption peak above this temperature (HT peak; Fig. 6). The low-temperature (LT) desorption peak, observed at 180 °C, corresponds to weakly bound NH_3,[60] and has been previously assigned either to NH_3 molecules solvating the NH_4^+ ions (*e.g.*, in $N_2H_7^+$ dimers) or to NH_3 desorbed from Lewis sites;[59,61] however, its identification is still a matter of controversy and its participation in the SCR reaction is ambiguous.[62] According to the desorption temperature observed for weakly bound NH_3 (180 °C), it appears that these species don't play any role in the present study; NH_3 adsorption was carried out at 250 °C for the *in situ* FTIR studies, so weakly bound NH_3 molecules are unlikely to be present on the catalyst surface at this temperature. Additionally, the high-temperature (HT) desorption peak, in the temperature range of 250–450 °C, is considered to be due to strongly bound NH_3, arising from protonated NH_3 formed over the Brønsted acid sites.[60]

After Cu^{2+}-exchange, the NH_3-TPD profile of Cu-SSZ-13(67) shows the presence of an extra desorption peak (IT peak) at 320 °C, attributed to NH_3 adsorbed over the Cu^{2+} sites, demonstrating that Cu^{2+}-exchange provides additional adsorption sites for NH_3, and consequently a reduction in the total number of Brønsted acid sites.[61] Accordingly, a significant decrease in the intensity of the HT peak is observed, together with a shift in the peak maximum to higher temperatures, indicating, as expected, a higher acid strength of the remaining Brønsted sites. Moreover, the broadening of the HT peak after ion exchange suggests an increase in heterogeneity of these sites after Cu^{2+}-exchange, with acid sites of varying strength being present.

In the case of the Cu-SSZ-13(100) zeolite, the higher Cu^{2+} loading is evidenced by a more pronounced increase in the intensity of the IT peak. However, despite the fact the maximum cation exchange level of the zeolite has been reached, the NH_3-TPD profile still shows an intense desorption peak at high temperatures, supporting the notion that some of the Cu^{2+} ions are present as monovalent complexes, for which Al pairs are not required for achieving charge balance. Nevertheless, the HT peak decreases in intensity, and is displaced slightly to higher temperatures, thus indicating a reduction in the number of the Brønsted sites accompanied by a small increase in their strength. This effect could be explained due to both an increase in the Cu^{2+} loading and the dealumination of the zeolitic framework that takes place during the consecutive exchanges with Cu^{2+}.

NH_3 availability and reactivity in CHA-type zeolites

The evolution of the different types of NH_3 species during SCR (250 °C; 1000 ppm NO and 5% O_2) was followed as a function of time by *in situ* FTIR, as outlined in Fig. 7 and 8. The results obtained for the Cu-SSZ-13(67) zeolite, show different reactivities for NH_3 species under SCR conditions; the spectrum recorded after 4 min (Fig. 7b) shows the disappearance of the NH_3 species adsorbed over Cu^{2+} ions to be almost complete, whereas the NH_4^+ ions formed over the Brønsted acid sites remain. The results are therefore consistent with those recently reported.[14,17]

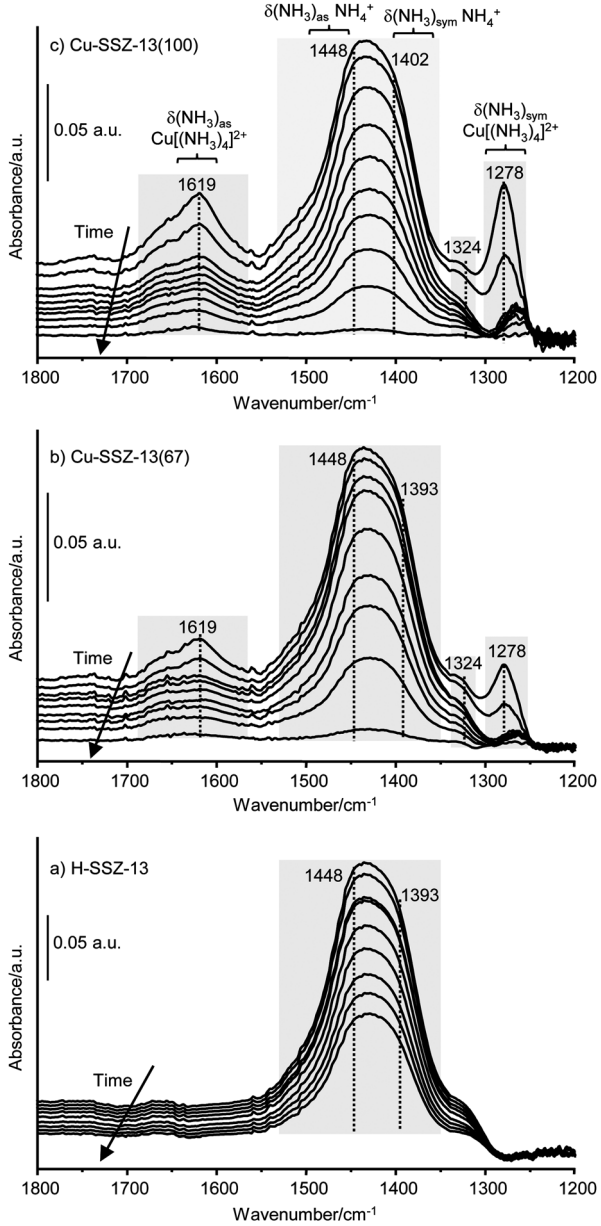

Fig. 7 NH_3 species reactivity during SCR (250 °C; 1000 ppm NO and 5% O_2) on H-SSZ-13 (a) and Cu-SSZ-13(67) (b) zeolites at 0 s, 35 s, 4 min, 1 h, 2 h, 3 h, 4 h, 5 h and 6 h of reaction time; and Cu-SSZ-13(100) (c) zeolite at 35 s, 2 min, 3 min, 4 min, 7 min, 9 min, 11 min, 14 min and 20 min of reaction time. Note the presence of at least two different NH_3 species: NH_4^+ ions (1448 and 1393 cm^{-1}) and $Cu[(NH_3)_4]^{2+}$ complexes (1619 and 1278 cm^{-1}).

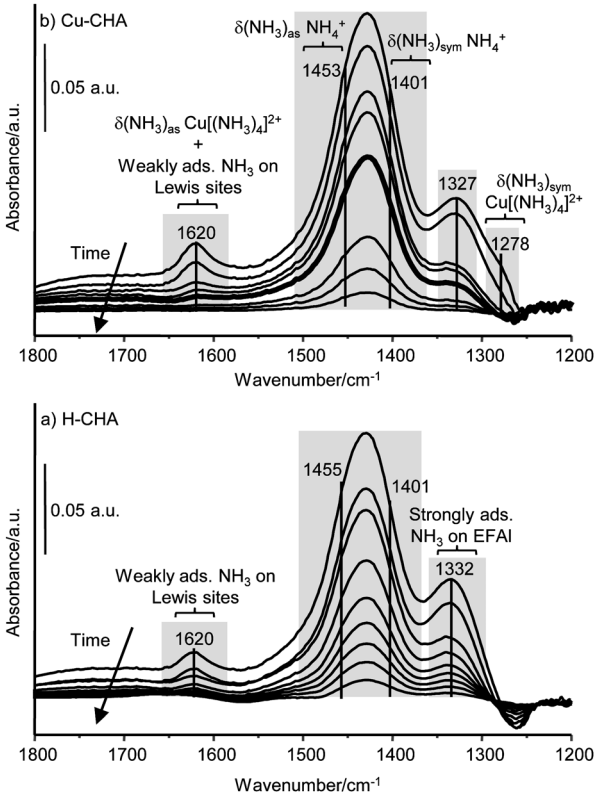

Fig. 8 NH_3 species reactivity during SCR (250 °C; 1000 ppm NO and 5% O_2) on H-CHA (a) and Cu-CHA (b) zeolites at 0 s, 35 s, 4 min, 1 h, 2 h, 3 h, 4 h, 5 h and 6 h of reaction time. Note the presence of at least three different NH_3 species: NH_4^+ ions (1455 and 1401 cm^{-1}), $Cu[(NH_3)_4]^{2+}$ complexes (1620 and 1278 cm^{-1}) and NH_3 coordinated with extra-framework Al (EFAl) species (1620 and 1332/1327 cm^{-1}).

Interestingly, the disappearance of NH_4^+ ions is much slower for the H-form zeolite, as evidenced by the spectrum recorded after 6 h (Fig. 7a). The reaction of NH_4^+ species is complete for the Cu-SSZ-13(67) zeolite after 6 h, while for the H-SSZ-13 zeolite the reaction takes more than 8 h, demonstrating the important role of the Cu^{2+} Lewis sites in the SCR reaction. These results suggest that the NH_4^+ ions formed at Brønsted acid sites barely contribute to the SCR process and may not be indispensable for the NH_3-SCR reaction, but function predominantly as NH_3 storage sites, as previously indicated.[12–14] This is likely to prove problematic at elevated temperatures (*e.g.*, temperature spikes), where NH_4^+ will be released (NH_3 slip) or else combusted (unexpected NO_x/N_2O release). Therefore, a reduced number of Brønsted sites would be favourable for the NH_3-SCR reaction.

Importantly, in the case of the Cu-SSZ-13(100) zeolite (Fig. 7c), the disappearance of NH_4^+ species is comparatively much faster than for Cu-SSZ-13(67), being complete after just 20 min of reaction. This result indicates that the availability of NH_4^+ ions can be particularly improved by submitting the zeolite to repeated exchanges with Cu^{2+}, most likely related with a modification of the acid strength and distribution of the acid sites during the repeated exchanges (see below). Since the differences in the chemical composition of the zeolites are not very pronounced (see Table 1), the enhanced reactivity of NH_4^+ ions cannot be definitively attributed to the higher amount of Cu present or the higher Si/Al ratio. Moreover, in view of the very low amounts of CuO detected within this sample (see ESI;† Fig. S7 and S8 and Table S2), the presence of these species cannot be considered as a possible reason of the enhanced reactivity.

In contrast to the results obtained for SSZ-13 zeolites, the spectra recorded for the Al-rich CHA materials (see Fig. 8), with ~18% of EFAl species, reveal very similar reactivities of NH_4^+ ions for both the H-form and the Cu^{2+}-exchanged zeolite; after

5 h of reaction, the spectrum recorded for the Cu-CHA zeolite shows almost complete disappearance of the NH_4^+ ions, whereas for the H-CHA zeolite the reaction is complete after almost 6 h. Comparison of these results with those obtained for the H-SSZ-13 and Cu-SSZ-13 zeolites, shown in Fig. 7, suggests that EFAl species, with Lewis acid character, could have a positive influence in the reaction rate of NH_4^+ ions for the low silica CHA zeolites, enhancing the availability of NH_3 molecules for the reaction. It is generally accepted that thermal and hydrothermal treatments of zeolites commonly lead to the abstraction of lattice Al atoms to form extra-framework Al (EFAl).[63] Depending on the experimental conditions and the zeolite type, a large number of Al atoms can be released from the framework, along with an enhancement of the Lewis acidity.[63] This is of particular importance for the SCR reaction, since hydrothermal ageing is one the main deactivation mechanisms.[64] To our knowledge, the influence of EFAl species in NH_3-SCR has received little attention so far.[57,65–67] Previous studies using NaY zeolites showed faster reaction rates and improved selectivity for nanocrystalline NaY, attributed to the increased external surface area, concentration of silanol groups and EFAl species on the external surface.[57,65] Moreover, investigation of the activity of H-ZSM-5 showed an enhanced reaction rate after mild steaming, suggesting the participation of EFAl species in the catalytic process.[66] In contrast, studies with dealuminated mordenites indicated a site-blocking effect due to the presence of polymeric EFAl species, which limit the accessibility to the sites responsible of the catalytic activity.[67] The results here obtained suggest a positive influence of the presence of EFAl species for the low silica CHA zeolites however, further experiments need to be performed to reach definitive conclusions, using different CHA zeolites with similar Si/Al ratios and Cu loadings, as well as varying amounts of EFAl species.

As previously mentioned, the characterisation results obtained for the high silica Cu^{2+}-loaded SSZ-13 zeolites (see above) showed very little differences between the catalysts, so no definitive conclusions could be made about the improved reactivity of the NH_4^+ ions. In an attempt to determine the influence of the ion exchange treatments on the reactivity of NH_4^+ ions, the two Cu^{2+}-containing SSZ-13 zeolites were further characterised by SEM and N_2 adsorption measurements. Moreover, activity tests were carried out under standard SCR conditions, using a GHSV of 100 000 h^{-1}.

Again, the N_2 adsorption measurements showed very similar results (see ESI;† Table S3); both Cu^{2+}-loaded zeolites present a typical type I isotherm, corresponding to a fully microporous material, so that the presence of an additional mesopore system in Cu-SSZ-13(100) produced as a consequence of the framework dealumination is not a possible reason of the enhanced reactivity. Identical results were also obtained by SEM (see ESI;† Table S3), ruling out a possible change in the crystal size and/or morphology after Cu exchange. In contrast, the catalytic tests performed, presented in Fig. 9, show a substantial improvement in the low temperature activity for the Cu-SSZ-13(100) sample. Both Cu-loaded zeolites present a

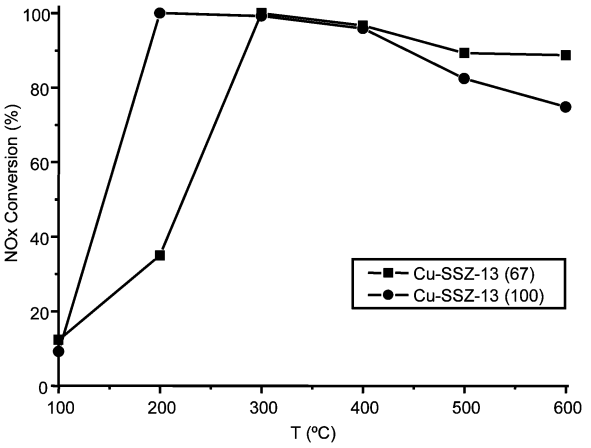

Fig. 9 NO_x conversion for Cu-SSZ-13(67) and Cu-SSZ-13(100) at different temperatures, using a GHSV of 100 000 h^{-1} and a feed composition of 1000 ppm NO, 1000 ppm NH_3 and 5% O_2.

notable activity over a wide temperature window however, in the case of the Cu-SSZ-13(100) zeolite, there is an important enhancement in NO conversion at low temperatures, from 30% in Cu-SSZ-13(67) to 100% in the Cu-SSZ-13(100) at 200 °C. A more pronounced drop in activity is found at temperatures up to 400 °C, attributed to the oxidation of NH_3 at high temperatures.[68] Clearly, these results are in contrast with those obtained by Kwak *et al.* for a series of Cu-SSZ-13 zeolites with different ion exchange levels;[69] just a slight increase in the activity at 200 °C was observed by increasing the ion exchange level from 20 to 40%, remaining almost constant at loadings above 40%. We note however, that the zeolites employed were synthesized by a different method, presenting a higher activity at 200 °C (~70%).[69] Therefore, the results here obtained give strong support to the idea that the enhanced reactivity is not related with the higher Cu loading of the Cu-SSZ-13(100) zeolite. In fact, similar results were recently reported by Martinez-Franco *et al.*, using Cu-SSZ-13 zeolites synthesized by one-pot methods.[70] The authors observed very different catalytic activities for Cu-SSZ-13 zeolites presenting the same chemical composition and similar crystal size, and pointed out a possible influence of the synthesis method, which could affect the Al distribution.[70]

Though work is in progress to shed further insight in the reasons behind the results here presented for the Cu-SSZ-13(100) zeolite, both the improved reactivity of NH_4^+ ions and the high activity at low temperatures could be indeed related to a different acid site distribution within the zeolitic crystals, leading to an enhanced NH_3 availability under SCR conditions. It is commonly accepted that Al atoms are not evenly distributed within the zeolite framework and that the probability of the presence of Al pairs decreases with the Al content. Hence, it is reasonable to think that the formation of $[Cu^{2+}(OH)^-]^+$ complexes is directly related with the Al content and its distribution within the zeolite crystals, as previously indicated.[21] Most likely, a particular Al distribution is achieved for the Cu-SSZ-13(100) zeolite crystals upon the consecutive exchanges

with Cu^{2+} (as well as the repeated calcinations), favouring the formation of $[Cu^{2+}(OH)^{-}]^{+}$ species and possibly influencing the acidic properties of the zeolite. It is known that the acid strength of the Brønsted sites is strongly influenced by the site location, but also by the Cu distribution; *i.e.* metal cations are considered as electron acceptors, so a Brønsted site located close to the metal cation becomes electron deficient, thus becoming a strong Brønsted site. Therefore, both Al and Cu distribution may have an important influence on the acidic strength of the Brønsted acid sites present in the Cu-SSZ-13(100) zeolite, enhancing the availability of NH_4^+ ions at low temperatures. Little information about the influence of exchange treatments on the acidic properties is available in the literature, so investigations are now being carried out to understand the influence of the different exchange protocols on the acid site distribution of the zeolite.

Conclusions

To gain further insight into NH_3 storage, availability and reactivity in Cu-Chabazite-based NH_3-SCR systems, the type and nature of NH_3 species adsorbed on CHA-type zeolites and their evolution under standard SCR conditions have been investigated by combining *in situ* FTIR spectroscopy with theoretical calculations. As catalysts, five CHA-type zeolites, with different populations of acid sites, have been used.

The zeolite samples under investigation have been characterised by several techniques, including chemical analysis, ^{27}Al MAS NMR, XRD, UV-Vis-NIR DRS or EXAFS. Additionally, the acid sites of the zeolites have also been characterised by combining FTIR measurements of the dehydrated samples (activated under O_2 flow) with theoretical calculations of vibrational frequencies. In particular, the results obtained for the Cu-SSZ-13(100) zeolite, with 100% of ion exchange degree, indicate that not all the Cu^{2+} ions are balancing the negative charge created by Al pairs, being also probably present in the form of monovalent $[Cu^{2+}(OH)^{-}]^{+}$ complexes, as previously observed by FTIR using CO and NO as probes[21] and hence resulting in an incomplete reduction in the number of Brønsted acid sites.

The most important conclusions reached in the present work are listed below as follows:

• Three different types of NH_3 species can be distinguished within Cu-Chabazite zeolites at 250 °C. They include NH_4^+ ions, resulting from NH_3 protonation over the Brønsted acid sites, $[Cu(NH_3)_4]^{2+}$ complexes formed on the Cu^{2+} Lewis sites and, when present, NH_3 adsorbed on EFAl species. Furthermore, NH_3 molecules could be also physisorbed or weakly adsorbed at low temperatures (<200 °C), although these species most likely do not play any role in the present study. These results are in contrast to those obtained in a previous work,[17] which showed the formation of only two reacting NH_3 species at 200 °C.

• The NH_4^+ ions formed on the Brønsted acid sites react very slowly in comparison to NH_3 coordinated to the Cu^{2+} ions and are likely to contribute little to the standard NH_3-SCR process. Therefore, Brønsted acid sites may not be indispensable, but act merely as NH_3 storage sites, as previously indicated by other research groups.[12–14] This could have serious implications, especially at elevated temperatures, where NH_4^+ ions are likely to become released (NH_3 slip) or else combusted (unexpected NO_x/N_2O release). Consequently, it is believed to be of particular importance to control NH_3 storage capacity to a level suitable to achieve high NO_x conversions, but not so high that it will lead to NH_3 slip at high temperatures; *i.e.* a reduced number of Brønsted sites, but with an optimal distribution and acid strength.

• The availability/reactivity of NH_4^+ ions can be however, notably improved by submitting the SSZ-13 zeolite to repeated exchanges with Cu^{2+}, leading to a substantial increase in the reaction rate of NH_4^+ species, together with an important enhancement in the low temperature activity of the zeolite, as demonstrated in Cu-SSZ-13(100). These differences are attributed to a particular Al and Cu distribution within the zeolite, favouring the formation of $[Cu^{2+}(OH)^{-}]^{+}$ species and influencing the acid strength of the remaining Brønsted sites. Within this context it has to be mentioned that the presence of EFAl species, with Lewis acid character, could also have a positive influence on the reaction rate of the NH_4^+ ions, as suggested by the low silica CHA zeolites, though more experiments are required to draw any firm conclusions.

Acknowledgements

This research was carried out under the Project number M.23.7.08301 in the framework of the Research Program of the Materials innovation institute M2i (www.m2i.nl). The authors would like to than NWO/FWO for DUBBLE beam time and Sachem inc. for kindly providing the template (Zeo-Gen2825) used in the synthesis of SSZ-13. Frank Mertens and Bart Wieland of DAF Trucks (Eindhoven, The Netherlands) are also thanked for their useful discussions and advice. This work was also supported by the Fund for Scientific Research Flanders (FWO), the Research Board of Ghent University (BOF) and from the European Research Council (ERC) under the European Community's Seventh Framework Programme [FP7(2007-2013) ERC grant agreement number 240483] and BELSPO in the frame of IAP P7/05. Computational resources and services used in this work were provided by the Stevin Supercomputer Infrastructure of Ghent University.

Notes and references

1 S. Brandenberger, O. Kröcher, A. Tissler and R. Althoff, *Catal. Rev. Sci. Eng.*, 2008, **50**, 492.
2 U. Deka, I. Lezcano-Gonzalez, B. M. Weckhuysen and A. M. Beale, *ACS Catal.*, 2013, **3**, 413.
3 J. H. Kwak, R. G. Tonkyn, D. H. Kim, J. Szanyi and C. H. F. Peden, *J. Catal.*, 2010, **275**, 187.
4 D. W. Fickel, E. D'Addio, J. A. Lanterbach and R. F. Lobo, *Appl. Catal., B*, 2011, **102**, 441.
5 S. T. Korhonen, D. W. Fickel, R. F. Lobo, B. M. Weckhuysen and A. M. Beale, *Chem. Commun.*, 2011, **47**, 800.

6 U. Deka, I. Lezcano-Gonzalez, S. J. Warrender, A. L. Picone, P. A. Wright, B. M. Weckhuysen and A. M. Beale, *Microporous Mesoporous Mater.*, 2013, **166**, 144.
7 D. W. Fickel and R. F. Lobo, *J. Phys. Chem. C*, 2010, **114**, 1633.
8 U. Deka, A. Juhin, E. A. Eilertsen, H. Emerich, M. A. Green, S. T. Korhonen, B. M. Weckhuysen and A. M. Beale, *J. Phys. Chem. C*, 2012, **116**, 4809.
9 R. Q. Long and R. T. Yang, *J. Am. Chem. Soc.*, 1999, **121**, 5595.
10 R. Q. Long and R. T. Yang, *J. Catal.*, 2002, **207**, 224.
11 J. Eng and C. H. Bartholomew, *J. Catal.*, 1997, **171**, 27.
12 S. Brandenberger, O. Kröcher, A. Wokaun, A. Tissler and R. Althoff, *J. Catal.*, 2009, **268**, 297.
13 Z. Liu, P. J. Millington, J. E. Bailie, R. R. Rajaram and J. A. Anderson, *Microporous Mesoporous Mater.*, 2007, **104**, 159.
14 D. Wang, L. Zhang, K. Kamasamudram and W. S. Epling, *ACS Catal.*, 2013, **3**, 871.
15 Y. Zhao, J. Hu, L. Hua, S. Shuai and J. Wang, *Ind. Eng. Chem. Res.*, 2011, **50**, 11863.
16 K. Kamasamudram, N. W. Currier, X. Chen and A. Yezerets, *Catal. Today*, 2010, **151**, 212.
17 H. Zhu, J. H. Kwak, C. H. F. Peden and J. Szanyi, *Catal. Today*, 2013, **205**, 16.
18 J. Wang, T. Yu, X. Wang, G. Qi, J. Xue, M. Shen and W. Li, *Appl. Catal., B*, 2012, **127**, 137.
19 S. C. Larsen, A. Aylor, A. T. Bell and J. A. Reimer, *J. Phys. Chem.*, 1994, **98**, 11533.
20 G. T. Palomino, P. Fisicaro, S. Bordiga, A. Zecchina, E. Giamello and C. Lamberti, *J. Phys. Chem. B*, 2000, **104**, 4064.
21 F. Giordanino, P. N. R. Vennestrøm, L. F. Lundegaard, F. N. Stappen, S. Mossin, P. Beato, S. Bordiga and C. Lamberti, *Dalton Trans.*, 2013, **42**, 12741.
22 M. Moliner, C. Franch, E. Palomares, M. Grill and A. Corma, *Chem. Commun.*, 2012, **48**, 8264.
23 S. Nikitenko, A. M. Beale, A. M. J. van der Eerden, S. D. M. Jacques, O. Leynaud, M. G. O'Brien, D. Detollenaere, R. Kaptein, B. M. Weckhuysen and W. Bras, *J. Synchrotron Radiat.*, 2008, **15**, 632.
24 M. Newville, *J. Synchrotron Radiat.*, 2001, **8**, 322.
25 N. Binsted, *EXCURV, CCLRC Daresbury Laboratory Computer Program*, 1998.
26 D. Massiot, F. Fayon, M. Capron, I. King, S. LeCalvé, B. Alonso, J.-O. Durand, B. Bujoli, Z. Gan and G. Hoatson, *Magn. Reson. Chem.*, 2002, **40**, 70.
27 J. VandeVondele, M. Krack, F. Mohamed, M. Parrinello, T. Chassaing and J. Hutter, *Comput. Phys. Commun.*, 2005, **167**, 103.
28 G. Lippert, J. Hutter and M. Parrinello, *Mol. Phys.*, 1997, **92**, 477.
29 G. Lippert, J. Hutter and M. Parrinello, *Theor. Chim. Acta*, 1999, **103**, 124.
30 A. D. Becke, *Phys. Rev. A: At., Mol., Opt. Phys.*, 1988, **38**, 3098.
31 C. T. Lee, W. T. Yang and R. G. Parr, *Phys. Rev. B: Condens. Matter Mater. Phys.*, 1988, **37**, 785.
32 A. Schafer, C. Huber and R. Ahlrichs, *J. Chem. Phys.*, 1994, **100**, 5829.
33 J. VandeVondele and J. Hutter, *J. Chem. Phys.*, 2007, **127**, 114105.
34 G. Bussi, D. Donadio and M. Parrinello, *J. Chem. Phys.*, 2007, **126**, 14101.
35 S. Nosé, *Mol. Phys.*, 1984, **52**, 255; S. Nosé, *J. Chem. Phys.*, 1994, **81**, 511.
36 T. Verstraelen, M. Van Houteghem, V. Van Speybroeck and M. Waroquier, *J. Chem. Inf. Model.*, 2008, **48**, 2414.
37 D. Lesthaeghe, P. Vansteenkiste, T. Verstraelen, A. Ghysels, C. E. A. Kirschhock, J. A. Martens, V. Van Speybroeck and M. Waroquier, *J. Phys. Chem. C*, 2008, **112**, 9186.
38 J. P. Merrick, D. Moran and L. Radom, *J. Phys. Chem. A*, 2007, **111**, 11683.
39 S. Bordiga, I. Roggero, P. Ugliengo, A. Zecchina, V. Bolis, G. Artioli, R. Buzzoni, G. Marra, F. Rivetti, G. Spano and C. Lamberti, *J. Chem. Soc., Dalton Trans.*, 2000, 3921.
40 A. Zecchina, S. Bordiga, G. Spoto, D. Scarano, G. Petrini, G. Leofanti, M. Padovan and C. Otero Arean, *J. Chem. Soc., Faraday Trans.*, 1992, **88**, 2959.
41 R. Buzzoni, S. Bordiga, G. Ricchiardi, C. Lamberti, A. Zecchina and G. Bellusi, *Langmuir*, 1996, **12**, 930.
42 J. Howard and J. M. Nicol, *J. Chem. Soc., Faraday Trans.*, 1989, **85**, 1233.
43 S. Bordiga, L. Regli, D. Cocina, C. Lamberti, M. Bjørgen and K. P. Lillerud, *J. Phys. Chem. B*, 2005, **109**, 2779.
44 S. Bordiga, L. Regli, C. Lamberti, A. Zecchina, M. Bjørgen and K. P. Lillerud, *J. Phys. Chem. B*, 2005, **109**, 7724.
45 K. Suzuki, G. Sastre, N. Katada and M. Niwa, *Phys. Chem. Chem. Phys.*, 2007, **9**, 5980.
46 M. Calligaris, G. Nardin, L. Randaccio and P. C. Chiaramonti, *Acta Crystallogr., Sect. B: Struct. Crystallogr. Cryst. Chem.*, 1982, **38**, 602.
47 C. Lo and B. L. Trout, *J. Catal.*, 2004, **227**, 77.
48 J. Dedecek, L. Capek, P. Sazama, Z. Sobalik and B. Wichterlova, *Appl. Catal., A*, 2011, **391**, 244.
49 L. Capek, J. Dedecek, P. Sazama and B. Wichterlova, *J. Catal.*, 2010, **272**, 44.
50 J. Dedecek, O. Bortnovsky, A. Vondrova and B. Wichterlova, *J. Catal.*, 2001, **200**, 160.
51 J. Dedecek and B. Wichterlova, *J. Phys. Chem. B*, 1997, **101**, 10233.
52 J. H. Kwak, H. Zhu, J. H. Lee, C. H. F. Peden and J. Szanyi, *Chem. Commun.*, 2012, **48**, 4758.
53 F. Gao, E. D. Walter, E. M. Karp, J. Luo, R. G. Tonkyn, J. H. Kwak, J. Szanyi and C. H. F. Peden, *J. Catal.*, 2013, **300**, 20.
54 F. Goltl, R. E. Bulo, J. Hafner and P. Sautet, *J. Phys. Chem. Lett.*, 2013, **4**, 2244.
55 F. Goltl and J. Hafner, *J. Chem. Phys.*, 2013, **136**, 064504.
56 S. Kieger, G. Delahay, B. Coq and B. Neveu, *J. Catal.*, 1999, **183**, 267.
57 S. Elzey, A. Mubayi, S. C. Larsen and V. H. Grassian, *J. Mol. Catal. A: Chem.*, 2008, **285**, 48.
58 A. Jentys, G. Warecka and J. A. Lercher, *J. Mol. Catal.*, 1989, **51**, 309.

59 M. Niwa, S. Nishikawa and N. Katada, *Microporous Mesoporous Mater.*, 2005, **82**, 105.
60 E.-Y. Choi, I.-S. Nam and Y. G. Kim, *J. Catal.*, 1996, **161**, 597.
61 G. V. A. Martins, G. Berlier, C. Bisio, S. Coluccia, H. O. Pastore and L. Marchese, *J. Phys. Chem. B*, 2008, **112**, 7193.
62 A. Sultana, T. Nanba, M. Sasaki, M. Haneda, K. Suzuki and H. Hamada, *Catal. Today*, 2011, **164**, 495.
63 R. D. Shannon, K. H. Gardner, R. H. Staley, G. Bergeret, P. Gallezot and A. Auroux, *J. Phys. Chem.*, 1985, **89**, 4778; A. Poppl, T. Rudolf and D. Michel, *J. Am. Chem. Soc.*, 1998, **120**, 4879.
64 J. H. Kwak, D. Tran, S. D. Burton, J. Szanyi, J. H. Lee and C. H. Peden, *J. Catal.*, 2012, **287**, 203.
65 G. Li, C. A. Jones, V. H. Grassian and S. C. Larsen, *J. Catal.*, 2005, **234**, 401.
66 S. A. Stevenson, J. C. Vartuli and S. B. Sharma, *J. Catal.*, 2002, **208**, 106.
67 M. Lezcano, A. Ribotta, E. Miro, E. Lombardo, J. Petunchi, C. Moreaux and J. M. Dereppe, *J. Catal.*, 1997, **168**, 511.
68 S. M. Jeong, S. H. Jung, K. S. Yoo and S. D. Kim, *Ind. Eng. Chem. Res.*, 1999, **38**, 2210.
69 J. H. Kwak, D. Tran, J. Szanyi, C. H. F. Peden and J. H. Lee, *Catal. Lett.*, 2012, **142**, 295.
70 R. Martinez-Franco, M. Moliner, J. R. Thogersen and A. Corma, *ChemCatChem*, 2013, **5**, 3316.

